Neurally-informed modelling unravels a single evidence accumulation process for choices and subsequent confidence reports

Grogan, J.P.[1,2]*†, Vermeylen, L.[3]†, Mannion, S.L.[1], McCabe, C.[1], Monakhovych, D.[1], Desender, K. [2]‡, & O'Connell, R.G.[1]‡

1. Trinity College Institute of Neuroscience, Trinity College Dublin, Ireland.
2. School of Psychology, Trinity College Dublin, Ireland.
3. Brain and Cognition, KU Leuven, Leuven, Belgium.

† the authors contributed equally to the work

‡ the authors jointly supervised the work

* Corresponding author: john.grogan@tcd.ie

Abstract

Subjective confidence in perceptual choices depends on computations occurring prior to and after choice commitment. However, the nature of these computations remains unclear. Current models disagree on two fundamental questions: what stopping-rule is applied to post-choice evidence sampling and to what degree do choice and confidence reports rely on shared versus distinct evidence accumulation processes? These models have proven difficult to dissociate because they often make similar behavioural predictions. Therefore, we used a neurally-informed modelling approach to jointly model initial choices and subsequent confidence reports while leveraging the additional constraints offered by human electrophysiological signatures of evidence accumulation. Participants made self-paced confidence reports after indicating perceptual choices on a random dot motion task, with stimulus presentation continuing during the interval between these responses. Model comparison showed that boundary-based stopping rules provided superior fits to the behavioural data than time-based stopping rules, as the latter could not account for relationships between confidence and confidence-RT. The behavioural fits were inconclusive when comparing models with a single evidence accumulation process dictating choices and confidence reports compared to models invoking a distinct post-choice process. However, the single-process model markedly outperformed the other models in terms of its ability to recapitulate the observed neural evidence accumulation patterns associated with choice confidence. Our study thus demonstrates that choice behaviour, subjective confidence, and associated neural decision signals can be jointly explained by a model invoking a single process of evidence accumulation with separate boundaries for the initial choice and subsequent confidence reports.

Introduction

Convergent evidence from neurophysiological recordings and mathematical models suggests that the evidence accumulation processes that underpin decision formation also contribute to our subjective sense of choice confidence. How and when those processes contribute to confidence remains unknown. In most human studies of choice confidence, participants are asked to make an initial categorical decision before reporting their confidence in that choice. These metacognitive reports tend to exhibit a number of systematic features including decreased confidence, slower confidence response times and increased change-of-mind probability following incorrect decisions (Feuerriegel et al., 2022; Resulaj et al., 2009; Van Den Berg et al., 2016). A variety of different models have been devised to account for this metacognitive behaviour, most of which invoke some form of post-choice evidence accumulation (Herregods et al., 2023; Moran et al., 2015; Pleskac & Busemeyer, 2010; Yu et al., 2015). While neurophysiological data do point to the operation of evidence accumulation processes in the interval between choice and metacognitive reports (Desender et al., 2021; Feuerriegel et al., 2022; Grogan et al., 2023; Ko et al., 2023; Murphy et al., 2015), there is ongoing uncertainty regarding several fundamental elements of this process.

The first of these elements is the stopping-rule that is applied to post-choice accumulation. Some models propose that post-choice accumulation continues for a fixed duration on each trial (with that duration varying across trials) after which the total accumulated evidence is compared against confidence criteria to generate explicit confidence ratings (e.g., Pleskac & Busemeyer, 2010). Alternative models propose that post-choice accumulation only ceases when the decision variable reaches an additional set of confidence boundaries that come into play once initial-choice commitment has been reached. These confidence boundaries usually collapse over time, ensuring that later confidence reports will be associated with lower confidence (Herregods et al., 2023; Moran et al., 2015). In addition to their stopping rules, the second element that the models disagree on is whether post-decisional evidence is incorporated into the same accumulation process that informed the initial choice (e.g., Pleskac & Busemeyer, 2010) or if it is evaluated within a distinct, independent process that is initiated once the choice has been made (e.g., Fleming et al., 2018; Murphy et al., 2015). For example, some studies have suggested that post-choice processes operate within a distinct reference frame, selectively accumulating evidence that an error has been made (Desender et al., 2021; Murphy et al., 2015).

The extent to which these models can be distinguished based solely on fits to behavioural data likely depends at least in part on whether and how the initial choice data are modelled. In keeping with the dominant models of perceptual choice (e.g. Drift Diffusion Model), most models of post-choice confidence assume that the initial choice is subject to a constant bound (Herregods et al., 2023; Moran et al., 2015; Pleskac & Busemeyer, 2010; Yu et al., 2015). This has the consequence that the same amount of evidence will have been accumulated by the time of commitment for all choices. As a result, models invoking a distinct post-choice accumulation process versus a single continued accumulation process tend to make similar predictions for confidence reports. However, there is now strong evidence from computational modelling and neurophysiology that observers collapse their choice boundaries as time elapses when choices must be reported under time pressure (Cisek et al., 2009; Evans et al., 2020; Katsimpokis et al., 2020; Kelly et al., 2021; Murphy et al., 2016). One consequence of having collapsing choice boundaries is that cumulative evidence at choice commitment can vary substantially and systematically across trials, which could provide a crucial additional constraint on models of *post-choice* confidence.

Our goal in the present paper was therefore to jointly model perceptual choices and subsequent self-paced confidence reports, and to compare models with different stopping-rules and post-choice accumulation processes. In addition to evaluating our models based on their fits to behaviour, we examined the extent to which they could recapitulate the observed pre- and post-choice dynamics of a well-validated neural signature of evidence accumulation known as the centro-parietal positivity (CPP). The CPP is a component of the human event-related potential that exhibits a gradual, evidence-dependent, RT-predictive build-up during decision formation, irrespective of whether the choice entails an immediate response, a delayed response, or no overt response at all (Kelly & O'Connell, 2013; O'Connell & Kelly, 2021; Rogge et al., 2022; Twomey et al., 2015). The CPP's pre-choice amplitude is modulated by contextual factors such as prior knowledge and time pressure, consistent with boundary adjustments identified by behavioural models (e.g., Kelly et al., 2021; Kohl et al., 2020; Steinemann et al., 2018). It declines as a function of time alongside choice accuracy, consistent with a collapsing bound effect (e.g., Kelly et al., 2021; Steinemann et al., 2018), and scales with explicitly reported confidence (Davidson et al., 2021; Gherman & Philiastides, 2015, 2018; Grogan et al., 2023; Herding et al., 2019; Tagliabue et al., 2019). Recent work has also established that the CPP continues to evolve after an initial choice report in a manner that predicts subsequent cued confidence reports (Grogan et al., 2023). To our knowledge, no previous study has examined the CPP's dynamics prior to self-paced confidence reports which may be essential in order to identify the stopping rules and evidence accumulation processes being implemented.

Results

Post-decision deadlines induce a Confidence-SAT

We recorded 128-channel EEG during a two-alternative random-dot motion discrimination task (see Figure 1). Participants reported the direction of coherent motion within a 1500ms deadline after which the stimulus remained on screen until participants rated their confidence on a 6-point scale ('certain left' to 'certain right'). In order to facilitate identification of the stopping rule for post-choice accumulation, we manipulated the time pressure applied to the post-choice confidence reports by varying the deadline for response (Speed Regime = 700ms; Accuracy Regime = 3000ms). We defined 'confidence' as the degree to which the confidence report aligned with the initially chosen alternative (e.g., after a left choice, the highest confidence level would be 'certain left' and the lowest confidence level would be 'certain right') and 'certainty' as the participant's confidence irrespective of whether or not they were endorsing the initial choice (e.g., after a left choice the highest certainty levels would be 'certain left' and 'certain right'). Response times (RT) for the confidence reports (confidence RT) were measured relative to initial choice RT. We also measured 'final-accuracy', the extent to which the confidence report indicated the correct motion direction; 'metacognitive sensitivity', the degree to which confidence ratings distinguished correct from incorrect responses (AUROC2, see Methods), and 'changes-of-mind', defined as trials on which the confidence report indicated that the incorrect alternative had initially been chosen.

As expected, initially correct choices had faster initial-RT (log RT: β=-0.1091, t(1,25331)=-8.2343, p<.0001), faster confidence RT (log confidence-RT: β=-0.0905, t(1,25331)=-4.2684, p<.0001), higher certainty ratings (β=0.1483, t(1,25331)=7.0579, p<.0001), higher confidence ratings (β=0.2607, t(1,25192)=8.4610, p<.0001), as well as fewer changes-of-mind (logistic regression: β=-0.7821, t(1,25323)=-33.6550, p<.0001). Participants reported their confidence more quickly in the Speed Regime (Figure 1d; single-trial mixed-effects regression on log(confidence-RT): β=-0.3494, t(1,25331)=-4.9135, p<.0001) and with lower final-accuracy (Figure 1e; logistic regression: β=-0.0408, t(1,25331)=-2.8443, p=.0045). Overall confidence ratings were not significantly affected by the speed pressure manipulation (Figure 1g; β=-0.0162, t(1,25224)=-1.0173, p=.3090) but there was

a significant reduction in certainty (Figure 1h; β=0.0637, t(1,25331)=-2.4627, p=.0138). Although the speed-pressure manipulation was only applied to the post-choice confidence reports, this nevertheless resulted in a slight decrease in initial RT (Figure 1b) and accuracy (Figure 1c), although only the effect on RT reached statistical significance (single-trial regression of log(RT): β=-0.1196, t(1,25331)=-3.7660, p=.0002; logistic regression on accuracy, β=-0.0187, t(1,25331)=-1.3342, p=.1822). In addition, there was a significant reduction in the frequency of changes-of-mind in the Speed Regime (Figure 1i; logistic regression: β=-0.1481, t(1,25331)=-6.0496, p<.0001); as changes-of-mind are usually corrective, this explains the lower final-accuracy in the Speed regime, as initial-errors were not corrected as often. Despite there being no overall reduction in confidence, metacognitive sensitivity was significantly reduced in the Speed Regime (Figure 1f; aggregate level regression: β=-0.3630, t(1,26)=-4.2433, p=.0002), replicating the findings of Herregods et al. (2023).

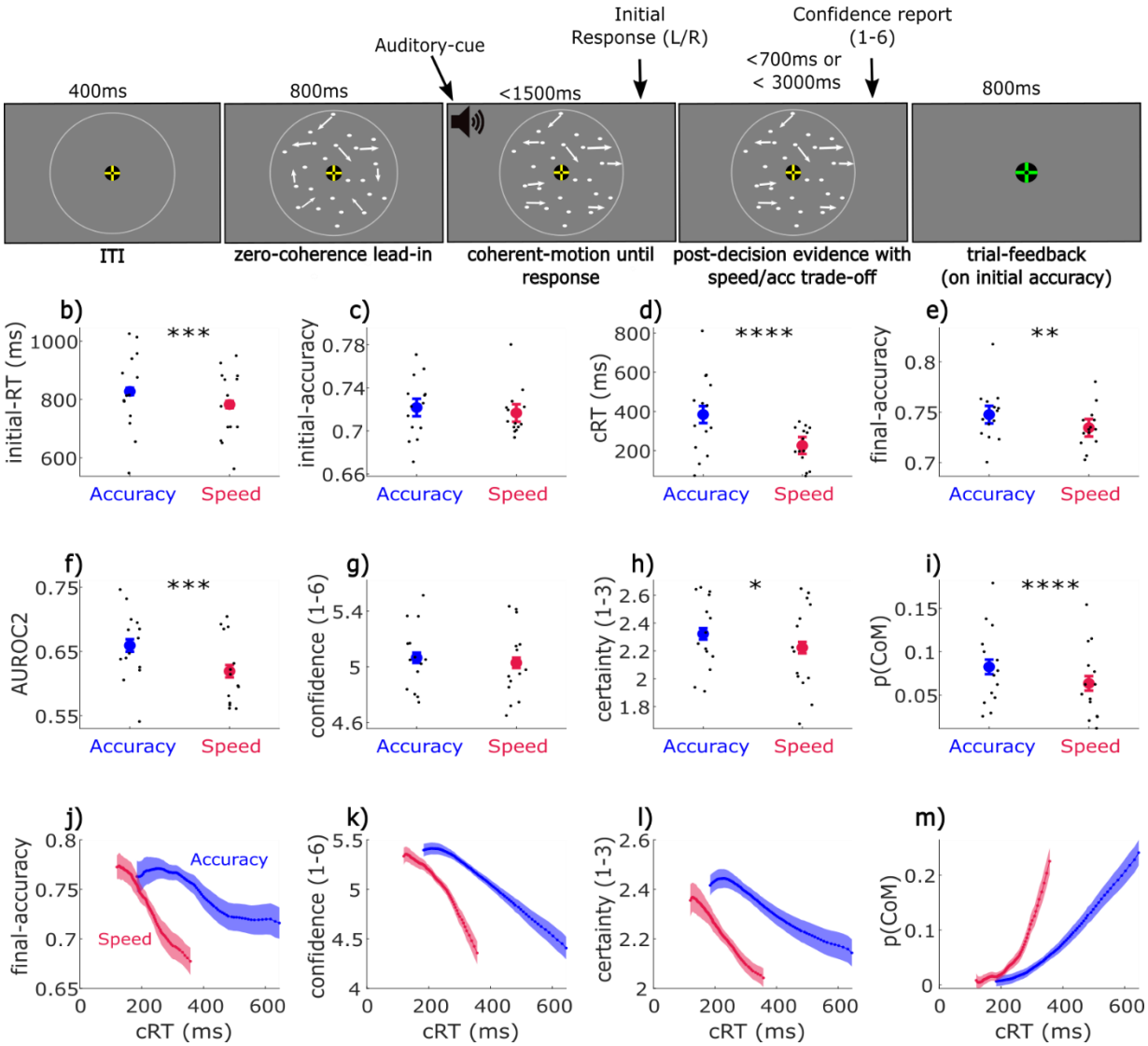

Figure 1. Task design and Speed-pressure effects on behaviour. *a) Random-dot motion task with zero-coherence lead-in, before a 1500ms deadline for an initial left/right choice. Moving dots with the same coherence remain on the screen as post-decision evidence, for either 700ms or 3000ms (blocked design) to induce a post-decision speed-accuracy trade-off; participants must rate their confidence before this deadline. b-k) Behavioural results; blue/red dots show overall means with 95% confidence intervals, black dots show individual-participants' means, and black stars show the significance of the speed-pressure effect, see text for full statistics (*=p<.05, **=p<.01, ***=p<.001, ****=p<.0001). Speed-pressure significantly decreases initial RT (b), confidence-RT (cRT; d), final-accuracy (e), AUROC2 (f), mean certainty (h) and changes-of-mind (CoM) (i). It did not significantly decrease initial-accuracy (c) or mean confidence (f). j-m) Conditional plots showing sliding window analysis of speed-pressure effects. Within each person and condition, we took a sliding window of 20% of*

cRTs, from the 1st to the 80th percentile, and plot the mean y-axis value at the mean cRT for that percentile-window, across participants, with shading showing SEM. This measures the change in the y-axis measure over increasing percentiles of cRT, while accounting for individual differences in mean and range of cRTs. Slower cRTs were associated with lower final-accuracy (j), lower confidence (k), lower certainty (l) and more changes-of-mind (m), with steeper slopes in the Speed-pressure condition.

Additionally, we observed that longer confidence-RTs were associated with lower final-accuracy (β=-.1465, t(1,24329)=-9.272, p<.0001), lower confidence (β=-0.3887, t(1,25222)=-5.2321, p<.0001) and certainty ratings (β=-0.1663, t(1,25239)=-4.0614, p<.0001), and more changes-of-mind (β=1.0922, t(1,25329)=12.9930, p<.0001), and these relationships were stronger in the Speed Regime (speed-pressure*confidence-RT on final-accuracy: β=-0.0560, t(1,25239)=-3.5577, p=.0004; confidence: β=-0.0967, t(1,25222)=-3.0604, p=.0022; certainty: β=-0.0549, t(1,25329)=-2.0666, p=0.0388; changes-of-mind: β=0.2739, t(1,25329)=9.8300, p<.0001). This pattern is consistent with confidence reports being subject to collapsing boundaries.

Comparing Model fits to Choice and Confidence Reports

To better understand the cognitive and neural mechanisms underlying perceptual choices and subsequent confidence judgements we turned to evidence accumulation models. To this end, we used a two-stage fitting procedure where we first fit a variant of the DDM in which the decision boundaries were free to linearly decrease over time, and then incorporated those best-fitting parameters into models that were designed to also account for the final confidence reports. The initial choice data were well explained by the model (Figure 2a, Extended Data Figure 1) which identified a substantial degree of boundary collapse that was common to both confidence report Regimes as well as a small reduction in initial boundary height in the Speed Regime (Extended Data Table 1).

To investigate the mechanisms underlying post-decisional processing, we evaluated four classes of models (Figure 2, see Methods for details). In all models, post-decision evidence is accumulated by a decision variable (DV) whose level at the time of commitment to the confidence report is translated into a confidence rating by comparison against confidence-criteria. The models included free parameters to estimate the position of each of the confidence criteria, as well as a metacognitive noise parameter to capture trial-to-trial fluctuations in the mapping of the DV to these criteria. All models had separate pre- and post-decision drift rates and non-decision time parameters. Post-choice non-decision times were estimated separately for changes-of-mind and no-change responses, to capture motor execution costs of switching hands between choice and confidence responses for change-of-mind trials.

The four models were distinguished based on two key categories: Time or Boundary based stopping rules; and Single or Distinct pre- and post-decision processes (Figure 2). Time-based stopping rules allow post-decision accumulation to continue for a set amount of time on each trial, with that time being drawn from a gaussian distribution, while Boundary-based models have linearly collapsing upper and lower confidence boundaries that terminate the process when reached. In Single-process models the post-decision accumulation process takes the form of a continuation of the pre-choice process, and therefore the DV's proximity to the confidence boundaries at the time of initial choice commitment is determined by how much evidence has been accumulated up to that point. In Distinct-process models, the starting-point (and therefore proximity to the confidence boundaries) of the post-choice accumulation process is freely fit independent of the DV's level at initial choice commitment, and the post-choice accumulation process only represents evidence accumulated *after* the initial choice.

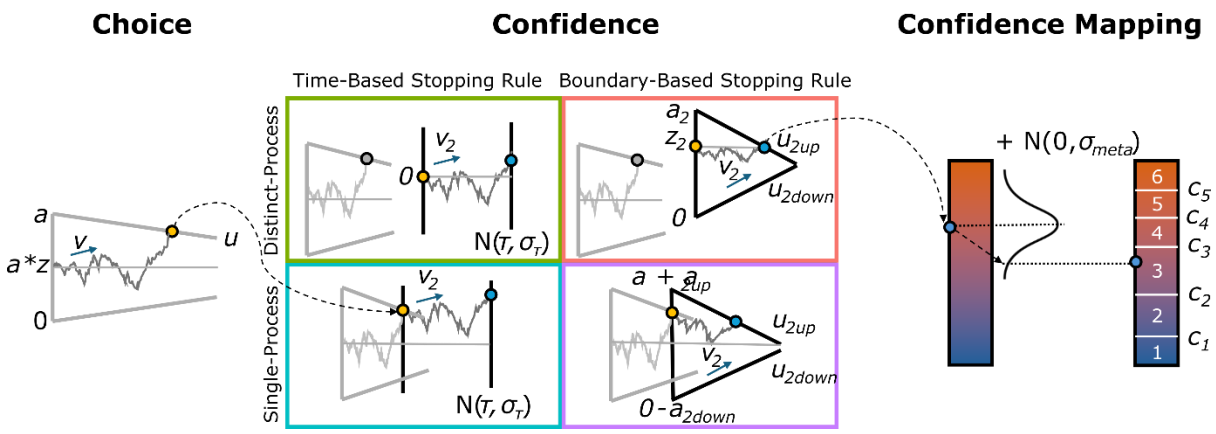

Figure 2. Overview of the Candidate Models. *(left) The initial choice was modelled using a drift diffusion model, where noisy evidence accumulates with a certain drift rate (v) until hitting a collapsing boundary (a; collapse rate controlled by u). Accumulation started at the unbiased point a*z. (middle) In Time-based models, the time of stopping was determined by a mean deadline time (τ) with some variability (σ_τ). In boundary-based models, the time of stopping was determined by collapsing boundaries, controlled by parameters related to confidence boundary heights (a_{2up} and a_{2down} for the Single-Process variant, a_2 and z_2 for the Distinct-Process variant), and corresponding collapse rates (u_{2up}, u_{2down}). Single-Process models evaluate post-decisional evidence relative to the initial reference frame used during choice formation (i.e., the unbiased starting point), while Distinct-Process models evaluate that evidence from a new reference frame (i.e., the freely estimated confidence starting point z_2). All post-decisional models included a parameter for the rate of post-decision accumulation (v_2). (right) Finally, in all models, evidence was translated into a six-point confidence scale using a metacognitive noise parameter (σ_{meta}) and five confidence criteria (c1 to c5). Non-decision components not displayed (see Methods).*

We estimated the post-decision parameters of the four models by minimizing a composite objective function that included the distribution of confidence RTs conditional on decision accuracy, the proportion of confidence ratings conditional on decision accuracy, and the proportion of confidence ratings conditional on confidence-RT quantiles (see Methods for details). Parameter and model recovery analyses showed that the four models are dissociable from each other using BIC model comparison, and that parameters of individual models are recoverable (see Methods/Model Fitting Procedure & Extended Data Figure 5). Each model was fit separately to data from both the Speed and Accuracy conditions. The two-stage fitting approach ensured that the models were able to capture the relevant behavioural patterns for both choice and confidence, while ensuring that the four models only differed in terms of their post-decisional processes.

Table 1. Goodness-of-fit metrics for the four classes of post-decisional models. *Values are mean scores over 14 participants in 2 conditions.*

Model	mean G2				Free Parameters	mean BIC
	cRT | accuracy	Confidence | accuracy	Confidence | cRT	Total		
Time-Distinct	95	**19**	112	226	11	301
Time-Single	97	20	125	242	11	317
Boundary-Distinct	**64**	43	**83**	**191**	13	**279**
Boundary-Single	67	31	96	194	13	282

Note. G2 values represent goodness of fit for different parts of the objective function that were minimized. BIC includes a penalty for the number of trials and number of free parameters. cRT = confidence RT. See Extended Data Tables 1-3 for fitted parameters.

Model comparison based on goodness-of-fit statistics accounting for model complexity indicated that Boundary-based models clearly outperformed the Time-based models (mean ΔBIC = 28.5; see Table 1). In particular, the collapsing Boundary models provided excellent fits for the shape of the confidence RT distributions (Figure 3A) and accurately captured that confidence RTs are much shorter than their choice RT counterparts (Figure 3C). The collapsing confidence bounds ensured

that slower confidence RTs were associated with less accumulated evidence and therefore lower certainty, whereas this association was completely missed by the Time-based models (Figure 3B). The two Boundary models could not be conclusively distinguished in terms of their fits to behaviour, with only a slight preference for the Distinct over Single process model (ΔBIC = 3; Figure 3B&C). Both models captured the speed pressure effects on confidence via faster collapse of the upper confidence boundary (Boundary-Distinct: $t(13) = -4.21$, $p = 0.0010$; Boundary-Single: $t(13) = -5.16$, $p = 0.0002$) but disagreed regarding the relative magnitude of pre- versus post-choice drift rate (with Boundary-Single indicating larger post-choice drift rate and Boundary-Double indicating larger pre-choice drift rates) and the role of non-decision time adjustments (with only Boundary-Single indicating a shortening of post-choice non-decision time for non-change-of-mind trials in the Speed Regime; see Extended Data Table 2-3 for full parameter results).

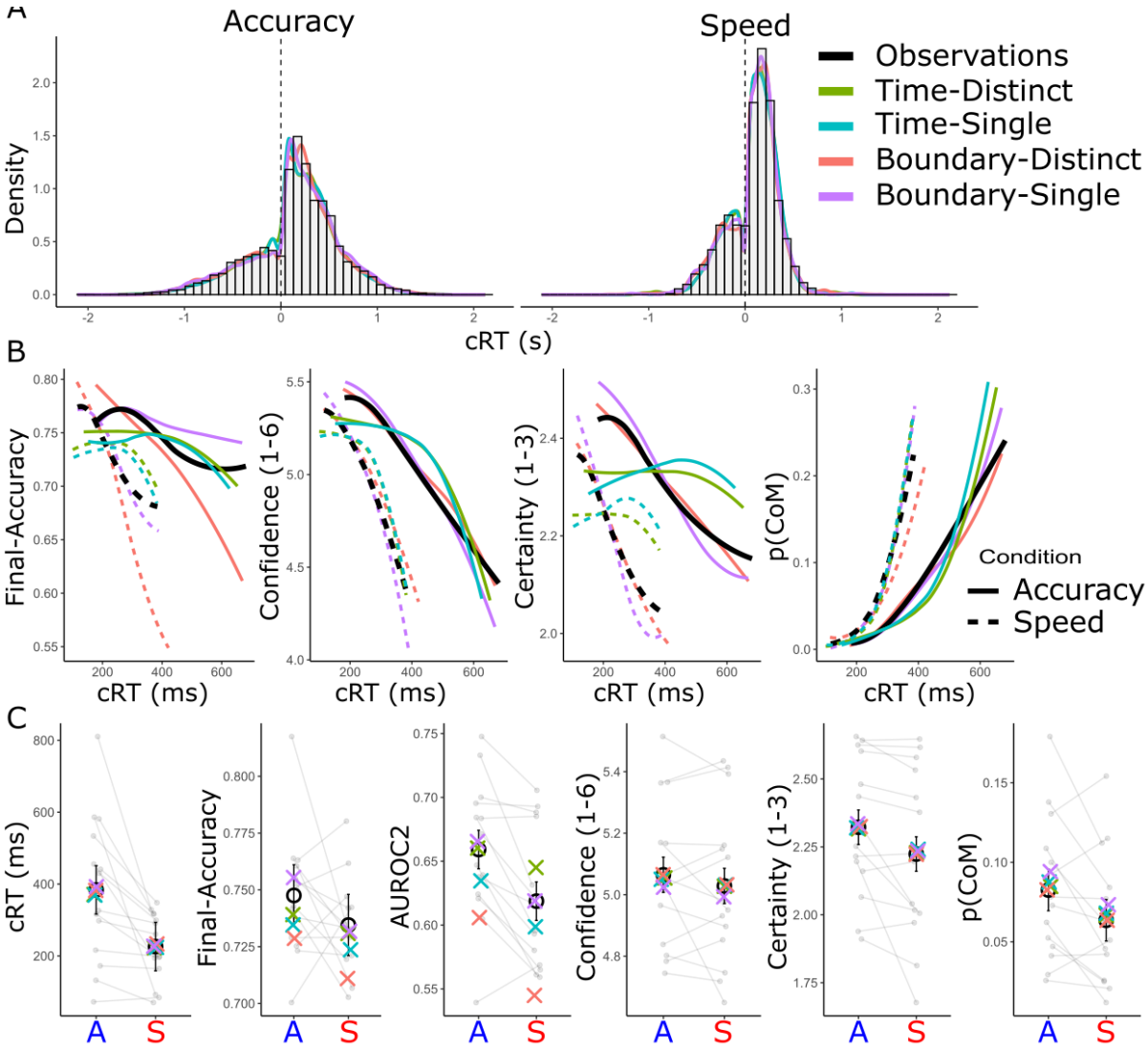

Figure 3. Model Fits to Behavioural Data Across Accuracy and Speed Conditions. *(A) Distributions of confidence response times (cRT) separate for correct (positive RTs) and incorrect (negative RTs) initial-choices in the Accuracy (left) and Speed (right) conditions. (B) final-accuracy, confidence, certainty, and change-of-mind (CoM) probability as a function of confidence-RT (cRT; smoothed using loess regression). (C) Mean cRT, final-accuracy, metacognitive sensitivity (AUROC2), confidence, certainty, and CoM probability for the Accuracy (A) and Speed (S) conditions. Error bars denote the within-subject 95% CI. Black histograms, lines, and points represent observed data, while coloured densities, lines and crosses represent the various model predictions. CoM=Change-of-mind.*

Although both Boundary models were nearly indistinguishable in terms of their overall fits, there were some qualitative differences in their predictions for behaviour. The Distinct-process variant benefits from greater flexibility due to the post-choice starting point being freely estimated, rather than being constrained by the DV's level at initial choice commitment. This allows the Boundary-Distinct model greater freedom to adjust its post-decisional dynamics to match the observed confidence patterns. However, this greater independence from the initial choice process comes at the cost of lower than observed metacognitive sensitivity (AUROC2) and final-accuracy (Figure 3C). In contrast, the starting-point and confidence boundaries of the Boundary-Single model are directly determined by the termination point of the initial decision, providing a better fit to final-accuracy and metacognitive sensitivity (Figure 3C) and the relationship between confidence-RT and final-accuracy (Figure 3B) but at the cost of a slightly worse replication of the confidence-RT distributions.

In order to further distinguish between the models, we leveraged our concurrently recorded EEG data to compare their ability to recapitulate the pre- and post-choice dynamics of a neural proxy of evidence accumulation; the Centro-Parietal Positivity (CPP).

Pre- and Post-choice neural evidence accumulation dynamics

In keeping with previous observations, the CPP showed a ramp-to-peak pattern leading up to the initial choice (Figure 4 - top row). The CPP is positive-going irrespective of which alternative the sensory evidence favours and, correspondingly, our previous work has shown that its amplitude at initial choice-commitment scales with the certainty of simultaneous confidence reports, irrespective of whether or not the confidence report indicates that an error had been made (i.e., Certainty rating; Grogan et al., 2023). Here we found that the same relationship holds when confidence is reported *after* the choice, with the CPP reaching significantly higher amplitudes both at the time of the initial choice and immediately prior to the final confidence report on trials rated with higher certainty (Figure 4A; black bars show significant clusters, $p<.05$). Note that confidence reports in our study were rather fast on average (Figure 3C), such that the choice-locked and confidence-locked CPP epochs overlap substantially, leading them to exhibit similar waveforms that are slightly shifted in time. We also found that speed-pressure affected the CPP but in the opposite direction expected from previous reports (e.g., Steinemann et al., 2018), reaching a higher amplitude before the initial and confidence responses in the Speed Regime (Figure 4C - top row; black bars show significant clusters, $p<.05$). Next, we compared the two Boundary models' ability to replicate these CPP effects.

Comparing Model and Neural Evidence Accumulation Time-courses

We used the best-fitting parameter values of each model to simulate evidence accumulation time courses. In keeping with previous work, since the CPP is positive-going irrespective of which alternative the evidence favours, we simulated the absolute value of accumulated differential evidence (e.g., Kelly et al., 2021). As detailed in Methods, the simulations for all four models incorporated several additional features to match known properties of brain signals like the CPP. These features included modelling a noisy baseline period before evidence onset, separating non-decision time into stimulus encoding and motor execution components, and incorporating a post-commitment signal decay (see Methods and Extended Data Figure 2). The simulation of the post-choice CPP differed for the Single- and Distinct-process models, reflecting their contrasting hypotheses regarding the reference frame for evidence accumulation. In the Single-process models, evidence accumulation continued seamlessly from the initial decision stage. In Distinct-process models, however, a separate post-decisional accumulation process was initiated; this new process used a novel starting point, which served as a new reflection point for calculating the absolute value of differential evidence.

To distinguish between the behaviourally similar Boundary-Single and Boundary-Distinct models, we compared the simulated DV to the observed CPP in two ways (simulations for the Time-based models can be found in Extended Data Figure 3). First, we examined average waveforms separately for different certainty ratings, change-of-mind occurrences, and speed Regimes; and second, we used time-based regression analyses to more formally disentangle the effects of certainty and changes-of-mind. Both models captured the qualitative patterns observed in the grand-average CPP, including a rise-to-peak before the initial decision, similar choice- and confidence-locked waveforms, and a decay to baseline that starts several hundred milliseconds before the confidence report (Figure 4). While both models did a good job of matching the average CPP dynamics, the Boundary-Single model was markedly better at reproducing the observed amplitude effects of Certainty (Figure 4A), with the Boundary-Distinct model predicting very small Certainty effects. The two models performed similarly well when accounting for changes-of-mind in the post-choice interval, although the Boundary-Distinct model provided a slightly superior match to the amplitude differences observed around the time of the initial choice (Figure 4B).

We also examined the extent to which the models could reproduce the effects of post-choice speed pressure on CPP amplitude but found that neither model agreed with the empirical data, with both predicting larger amplitudes for the Accuracy compared to the Speed condition (Figure 4C).

As certainty and changes-of-mind are partially correlated, we used regression analysis to compare the time intervals over which the empirical and simulated CPP encoded these variables. The beta-coefficients plotted in Figure 4D show the effects of Certainty, changes-of-mind, and their interaction, on the real or simulated traces at each time-point. The empirical data showed a rising effect of Certainty on CPP amplitude starting ~500ms before the initial response, which persisted until the confidence report. An effect of change-of-mind was also observed but it emerged much closer to the initial response and there was also a significant interaction between Certainty and change-of-mind that emerged prior to the initial response. Confirming the pattern shown by mean simulated DVs above, the Boundary-Single model was far better able to capture the time-course of the relationship between Certainty and amplitude than the Boundary-Distinct model. The models were not readily distinguishable based on their ability to capture changes-of-mind, with Boundary-Distinct models again providing a better match to the pre-choice data but Boundary-Single models better capturing the post-choice data. However, the Boundary-Single model again substantially outperformed Boundary-Distinct in capturing the Certainty by change-of-mind interaction time-course.

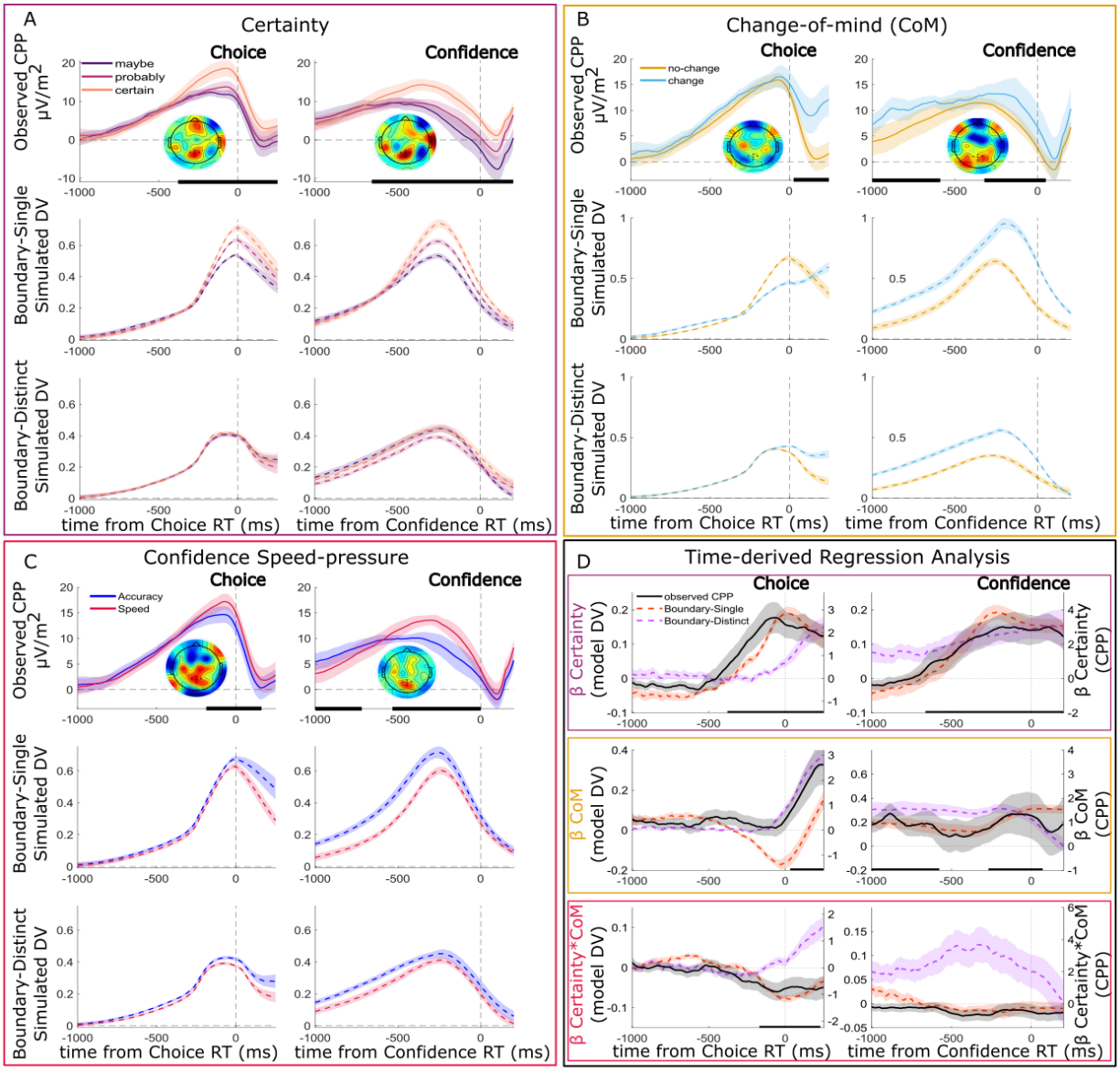

Figure 4. Observed CPP & Simulated Decision Variable, and Regression Analysis. *(A) Certainty Ratings. (B) Change of mind (CoM). (C) Speed Pressure. (D) Time-derived regression analyses. In panels A-C, the CPP is presented in the top rows, the simulated decision variable from the Boundary-Single model in the middle rows and the Boundary-Distinct model in the bottom rows. Left columns show choice-locked waveforms and right columns show confidence-locked waveforms. Choice-locked epochs end 250ms after initial response, which is just longer than the average median confidence-RT (243ms). Topography insets show the effects of each factor on mean observed EEG activity -150:-50ms before the initial choice or the confidence response (for Certainty, the difference is between Maybe and Certain ratings);lack dots show the CPP electrodes. (D) Time-derived Regression analyses, showing the beta-coefficients for Certainty, CoM and Certainty*CoM effects for the model DVs (left-axis) and CPP (right-axis). Solid black bars along the bottom show clusters of significant effects on the observed CPP (single-trial time-derived LME regression, with permutation testing and cluster-control of FWER at .05) and Error bars reflect the within-subject SEM.*

As a final step we considered the possibility that a Single accumulation process could be implemented by two distinct signals, one that accumulates evidence for the initial choice and another that is initiated upon commitment and which tracks updates to the DV based on post-choice evidence (Boundary-Update model; see Methods and Extended Data Figure 4). This implementation provided a poor match to the CPP data, predicting larger pre- and post-choice amplitudes for trials with lower certainty ratings (the absolute DV in the Boundary-Update model will increase on average irrespective of whether the cumulative evidence favours the chosen or unchosen alternative), suggesting one continuous accumulation process explains the data better.

Discussion

We adopted a neurally-informed modelling approach to identify a set of computational mechanisms that could jointly account for choice behaviour, subsequent self-paced confidence reports, and the pre- and post-choice dynamics of a neural signature of evidence accumulation. The results indicated that rather than post-choice accumulation being subject to an internally set deadline on each trial, it is instead terminated once the cumulative evidence reaches a collapsing upper or lower confidence boundary. While the behavioural modelling unequivocally favoured a boundary-based stopping rule for the final confidence reports, it was inconclusive on the question of whether post-choice evidence accumulation is simply a continuation of the process that informed the initial choice or whether it is the result of a new accumulation process. Here, evaluating the degree to which the models could recapitulate neural data not included in the fitting process played a pivotal role in distinguishing between these alternative accounts, with the single process model markedly outperforming those invoking a distinct post-choice process in matching the CPP's confidence-predictive dynamics before and after choices.

Theories of metacognition have long disagreed on the question of whether confidence is computed in parallel with, or subsequent to, choice commitment (Kiani & Shadlen, 2009; Pleskac & Busemeyer, 2010; Vickers, 1979). Here we examined this issue by pitting a model in which post-choice confidence reports arise from a continuation of the same evidence accumulation process that informed the initial choice (Boundary-Single) against models in which choice commitment triggers a new accumulation process (Boundary-Distinct). Similar to the second-order model of Fleming & Daw (2017), the Distinct models were blind to any variations in cumulative evidence at the time of the initial choice. This distinction between models could not be made in most previous studies since they have tended to assume fixed choice-boundaries, and therefore invariant cumulative evidence at the time of commitment to the initial choice (Herregods et al., 2023; Moran et al., 2015; Pleskac & Busemeyer, 2010). Here, our model identified a substantial degree of boundary collapse for the initial choice process. As a result, later choices tended to be associated with less cumulative evidence and therefore lower accuracy, certainty, and confidence. While adding collapsing choice-boundaries did not produce a clear-cut winner between these models in the behavioural fits, it did have a significant impact when comparing the models based on their simulated evidence accumulation time-courses. Only the Boundary-Single model was able to reproduce the positive relationship between CPP amplitude and certainty that emerged several hundred milliseconds before the initial choice and remained until the final confidence report. In contrast, the Boundary-Distinct model showed no pre-choice certainty effects and only small post-choice effects. Our modelling also considered the possibility of a post-choice accumulation process that is initiated at choice commitment, but which takes account of the evidence already accrued by adjusting its confidence boundaries (Boundary-Update). Here again, the model provided a poor match to the neural data, suggesting that not only is information shared between pre- and post-choice processes, but that it is encoded by a single continuous process rather than information transfer between two.

Our modelling results resolve an apparent divergence in previous empirical work regarding whether pre- or post-decision evidence feeds into the computation of confidence. Inspired by computational models of confidence positing an exclusively post-decisional locus of confidence (Pleskac & Busemeyer, 2010) much empirical work has shown how evidence presented after the choice causally affects the confidence reports (Charles & Yeung, 2019; Desender et al., 2021; Fleming et al., 2018; Moran et al., 2015; Rollwage et al., 2020). In seeming contrast, traces of confidence have been shown to emerge already early during the decision-making process (Dotan et al., 2018) and TMS pulses applied to right DLPFC as early as 200ms post-stimulus selectively increase confidence (Xue et

al., 2023). Although these observations are sometimes treated as opposing, they can all be accounted for within the context of the Boundary-Single model, which treats both the pre- and post-decision accumulation as informative for computing confidence. Thus, a key insight from our modelling is that the neural processes governing metacognitive representations of choice confidence are intimately tied to the processes that produce the choices themselves. Our neurally-informed model furnishes new ways of disentangling choice and metacognitive processes by specifying pre- and post- choice boundaries, drift rate, and non-decision time parameters while also estimating the mapping of evidence to specific confidence ratings. In so doing, our model has the potential to offer a more detailed account of inter-individual differences in metacognitive performance including those associated with clinical brain disorders.

There were however some features of the CPP that were not fully captured by our model, most notably its larger amplitude in the Speed Regime. This was an unexpected observation since previous studies that have applied speed-pressure to the *initial* choice have observed a lowering of pre-response CPP amplitudes (Kelly et al., 2021; Steinemann et al., 2018). One possible explanation is offered by the recent finding that asking participants to give post-decision confidence ratings resulted in slower and more accurate initial choices, along with a CPP that peaks earlier relative to the initial choice (Dou et al., 2024). This last observation suggests that post-choice confidence reporting may result in longer delays between initial choice commitment and response execution. Indeed, here too we observed that, on average, the CPP decayed back to baseline several hundred milliseconds prior to the final confidence report. It is possible that these delays are reduced and less variable in the Speed Regime resulting in a signal that is more closely time-locked to response execution and therefore larger in amplitude; correspondingly the Boundary-Single model identified a shorter post-choice non-decision time for non-change-of-mind trials in the Speed Regime. We did not fit variability parameters, to simplify the post-decision models, but future work could investigate whether the addition of non-decision time variability might enable the model to capture speed-pressure effects on the CPP.

Our behavioural and modelling results converge with those of a previous study using a similar task that separated speed-accuracy trade-offs (SAT) at the initial choice and confidence-report stages (Herregods et al., 2023). We replicated their observation that increasing speed pressure for confidence reports impairs metacognitive sensitivity without decreasing mean confidence ratings, as well as decreasing choice RT. One striking difference is that Herregods et al. (2023) observed significant confidence-SAT effects on the height of confidence-boundaries, whereas in the current work our confidence deadlines influenced the collapse rate of the confidence boundaries. This difference likely arises from different speed pressure manipulations; whereas we adjusted the response deadlines for the confidence reports, Herregods et al. (2023) instead instructed participants to prioritise speed or accuracy, without specifying a new deadline. These two SAT manipulations have been shown to affect initial boundary height and collapse rates differentially (Katsimpokis et al., 2020) and the same may be true for confidence boundaries.

While we have described the Boundary-Single model in terms of a single accumulation process that continues seamlessly after initial choice commitment, this model variant did identify some notable differences in pre- versus post-choice parameter estimates. As mentioned, non-decision times were shorter for non-change-of-mind trials in the Speed Regime and the model also indicated that post-choice drift-rates were substantially larger than pre-choice drift-rates. Some previous studies that modelled pre- and post-choice behaviour have reported a lower post-decision drift-rates (Bronfman et al., 2015; Desender et al., 2022; Talluri et al., 2021) which may arise from the fact that the

physical evidence was extinguished once the choice was reported in those studies. Here, the same evidence that was presented before the choice remained on screen until confidence was reported and our modelling suggests that an increased weighting was applied to the post-choice evidence. However, Herregods et al. (2023) reported higher post-choice drift rates despite also extinguishing the evidence after the initial choice, therefore more work is required to establish the origins of these effects, and a neurally informed approach will be useful in comparing mechanisms with similar behavioural predictions. Although not the focus of the current study, our model offers a useful framework for experimental manipulations probing post-choice changes to evidence sensitivity and phenomena such as confirmation bias (Mazor et al., 2022; Rollwage et al., 2020; Talluri et al., 2018).

Methods

Prior to commencing any data analysis, the study design, hypotheses, and planned analyses were pre-registered on Open Science Framework (https://osf.io/adctm).

Ethics

Trinity College Dublin ethics committee approved the study, and all procedures were performed in accordance with the Declaration of Helsinki and EU GDPR. Participants provided written consent before the start of the first session.

Participants

In order to collect a sufficient number of change-of-mind trials per participant (which are usually around 10% of trials in similar tasks), we used a large-trial number, small-N design, collecting 2160 trials per person across three testing sessions. Participants were aged 18-40 without psychiatric or neurological illnesses. In our pre-registration we specified a sample-size of 12-15 participants based on previous studies using similar tasks (Grogan et al., 2023; Walsh et al., 2024) but ultimately recruited 16 participants, as one participant had to be excluded prior to completing testing due to low accuracy during training, and another was excluded after indicating in their last testing session that they had misunderstood the instructions relating to the confidence ratings. The final dataset was therefore comprised of 14 participants (5 female & 9 male) with a mean age of 25 years (SD=4.3, range=20-36). They were paid €80-100 in total, including a performance-dependent bonus (see task details below).

Design

We used a within-subject design to test the effect of varying the deadline (relative to the initial choice report) for making post-choice confidence reports. This was implemented with a blocked-design, alternating blocks of long and short deadlines, with the condition order counterbalanced across participants via pseudo-randomisation.

Experimental Task

The task was a random-dot motion direction discrimination task designed in MATLAB (R2013b, www.mathworks.com) and Psychtoolbox-3 (Kleiner et al., 2007), and presented on a 1024x768 pixel monitor (100Hz refresh rate) approximately 60cm from the participant. Gaze and pupil diameter were recorded with an Eyelink 1000, following 9-point calibration at the start of each block, and drift-correction every 9 trials.

The task started with a central fixation cross and a white ring (10° diameter) on a grey background for 400ms, and then a cloud of 60 moving dots (0.15° diameter) appeared within an 8° diameter aperture. The dots initially moved with zero coherence for 800ms, to allow any visual-evoked potentials to reduce, before coherent motion to the left or right began (50% probability of each

direction). After this lead-in period, coherent motion began with a proportion of dots being displaced relative to their position 3 frames earlier, to give a dot speed of 6° per second, with the remaining dots displaced randomly. To remove ambiguity about the onset of coherent motion, and reduce premature responses, a beep (100ms, 500Hz, Hanning-tapered at edges to prevent clicks) was presented at coherence onset. Participants responded with their left/right thumbs (on buttons 'C' and 'N') to indicate the perceived direction, with a deadline of 1500ms. After a valid response, the dots remained moving at the same coherence until participants reported their confidence in the perceived direction on a 6-point scale with their fingers (certain/probably/maybe left using keys 1, 2 and 3 respectively, or maybe/probably/certain right using keys 8, 9, and 0). Participants were instructed that they could change their minds between initial and confidence responses, for instance responding 'left' initially and then 'maybe right'. We manipulated the deadline for this confidence-report, alternating blocks of trials with short (700ms, speed-pressure condition) or long (3000ms, accuracy-condition) deadlines while instructing the participants that the deadline for the initial choice always remained the same (1500ms). To continually remind participants which deadline applied on each trial, the fixation cross was coloured blue in long deadline blocks and yellow in short deadline blocks, and participants were also reminded of the change in deadline at the start of each block. The fixation cross changed colour at the end of a trial to indicate the accuracy of the initial response (green=correct, red=incorrect/early/late), and early or late initial-responses or late confidence-responses were given 'TOO FAST', 'TOO LATE' or 'confidence TOO LATE' feedback alongside a red fixation cross (feedback duration = 800ms). In each of 3 EEG sessions, participants completed 6 blocks of 120 trials, with a short break halfway through each block (2160 trials in total, 1080 per condition). Participants were reminded of the task instructions at the start of each session.

Prior to commencing the formal testing, a training session was conducted in which participants were first introduced to the different elements of the task and given time to practice and demonstrate to the researcher that they had understood the instructions. Training started out with 50% coherence until participants responded with >90% accuracy (initial-responses only, confidence-responses were not given here), and then coherence reduced in steps of 5% every 8 trials until it reached 10% coherence. Then the confidence-responses were introduced, and participants were given 30 trials to practice with the long (3000ms) deadline, and 30 trials with the short (700ms) deadline, using an easy coherence level based on their performance on the decreasing staircase. Following this, participants completed an additional block of 120 trials in which coherence was titrated using the QUEST procedure (Watson & Pelli, 1983) to achieve 70% initial choice accuracy (participants were still asked to provide post-choice confidence ratings but these did not inform the titration procedure). A further 30 trials were run to verify that participants were performing within 65-75% accuracy. If performance was outside this range, then coherence was manually adjusted and further 30 trial blocks were run until accuracy was within the desired range. In addition to this initial staircase procedure, initial choice accuracy was monitored throughout the formal testing and the coherence level was manually adjusted if participants' accuracy was not within 65-75%; this was only adjusted every second block, to ensure the coherence was the same for each pair of Speed and Accuracy blocks.

EEG recording & pre-processing

EEG was recorded with a BioSemi ActiveTwo system (Biosemi, Netherlands) at 1024Hz with a 128-channel cap and two VEOG electrodes on the left eye. Data were pre-processed with ERPLab (Delorme & Makeig, 2004) and custom MATLAB scripts. Each block's data were linearly detrended and low-pass filtered (40Hz FIR filter), and synchronised with the eye-tracking data with the EYE-EEG extension (Dimigen et al., 2011). EEG data were epoched from -1000:4000ms relative to coherence-

motion onset, and baseline-corrected to the mean voltage in the 200ms before the coherence onset. Channels were visually inspected for extreme variance and up to 10% of channels interpolated.

Trials were examined for artefacts from the 50ms before the start of the baseline period until 250ms after the confidence-report on each trial. Trials were rejected if they contained scalp voltage ±100µV, bipolar VEOG voltage ±200µV, saccades over 2° or eye-position drifting >4° from the fixation-cross (as detected by Eyelink), or initial RT <100ms or no valid initial or confidence responses. The mean number of trials per participant without artefacts was 1807 (SD=230.5, range=1371-2063).

Voltages were transformed into Current Source Density (Kayser & Tenke, 2006) using the default parameters. This sharpens the spatial focus of components and reduces the overlap of frontal components that can obscure confidence-related effects from centro-parietal components (Feuerriegel et al., 2022).

Due to the auditory beep coinciding with coherent motion onset, there was a strong auditory evoked potential evidence in the EEG data, which we removed with the RIDE algorithm (Ouyang et al., 2015) similar to previous work (Steinemann et al., 2018). This algorithm separates out a stimulus-locked component from a response-locked component and a third component not locked to either stimulus or response times. These components are generated for each electrode from an entire session's data and are fit over iterations to reduce the discrepancy with the data. Mean components are fit across each day's session separately, to allow for slight variations in the auditory evoked potential on each day, but across the speed and accuracy conditions. This gave one stimulus-locked component per session that was the same for all trials and both conditions, and thus does not affect the differences in potentials between the two conditions. The stimulus-locked component was removed from all trials and electrodes, and the baseline correction re-applied.

The CPP was measured as the mean of 5 centro-parietal electrodes which showed a positivity in the grand-average topographies from -170:-50ms before the initial-response.

Behavioural and Neural Analyses

Confidence was rated on a 6-point scale relative to the motion direction, which allowed for changes-of-mind between responses, and this was transformed to be relative to the initially-chosen direction, such that sticking with the same direction was rated as 4/5/6 for maybe/probably/certain non-change-of-mind, and change-of-mind responses were rated 3/2/1 for maybe/probably/certain change-of-mind. Thus, confidence measures participants' subjective perception that their initial choice was correct. We additionally calculate 'certainty' in the final choice, using the maybe/probably/certain label selected (1/2/3), regardless of whether this was a change-of-mind or not. Initial-RT is measured in milliseconds from the coherent motion onset, and confidence-RT is measured in milliseconds from the time of the initial response (no minimum confidence-RT threshold is applied). RTs were log transformed for statistical analysis. We additionally calculate the area under the ROC2 curve (AUROC2) to measure metacognitive sensitivity (Maniscalco & Lau, 2012); this measures how well subjective confidence-ratings track the objective accuracy of the initial choice.

To compare effects on behavioural variables, we used single-trial generalised linear mixed-effects regression for statistical analysis (using logistic regression for the binary variables of accuracy and change-of-mind). Predictor variables were z-scored to give standardised regression coefficients. The random-effects structures were picked using a forwards-selection method for each analysis separately (Matuschek et al., 2017), starting from a random intercept only and adding in terms in

order of their BIC improvement until likelihood ratio tests became non-significant or the model failed to converge. Interaction-term random effects were only included if all the main-effects within them had already been added.

Additionally, we ran a window-free analysis to compare effects on the CPP across all time-points, by running the single-trial linear mixed-effects regressions at each time-point, as described above. The same random-effects structure was used for all time-points, which was the one chosen using the selection method described above for the mean-amplitude within the -150:-50ms time-window. To generate p-values, we ran 5000 permutations, permuting rows of the design matrix (i.e., the predictors) within-participants, and calculating the proportion of permutations that had a cluster mass as or more extreme than the true t-values (Bullmore et al., 1999; Maris & Oostenveld, 2007), to give a two-tailed p-value with family-wise error rate controlled at .05. These permutation-tests are time- and computationally-intensive across many time-points and trials due to mixed-effects regressions being much slower than fixed-effects methods, so we used the lmeEEG toolbox (Visalli et al., 2024) to speed this up. This method first regresses out the random-effects at every time-point, by fitting the mixed-effects model, removing the random-effects, leaving behind the fixed-effects and residuals. This 'marginal EEG' data is then analysed with fixed-effects regressions using OLS (for both true-regressions and permutation-regressions), which gives almost identical results to running the full mixed-effects permutation testing, but much quicker (Visalli et al., 2024).

We set a minimum trial-number threshold for inclusion in the figures/analyses of 10 trials per condition (or combination of conditions as in the example above). Participants who had fewer than 10 trials per condition/combination were excluded from that particular condition, but included in all other conditions and analyses. Please note, the mixed-effects analyses used allow missing data for particular conditions.

When plotting CPP traces, the data were smoothed with a 100ms window moving-average.

Model Specification

We modelled the initial decision using a drift-diffusion process with linearly collapsing boundaries. Here, noisy evidence accumulation is approximated as a discrete-time random walk:

$$dx = v * dt + \sigma * dW \qquad (1)$$

where *dx* represents the change in evidence over the time step *dt* (set to 0.001s), *v* is the drift rate representing the average rate of evidence accumulation, and σ represents the within-trial diffusion noise, which was fixed to 1. *dW* represents an increment of a Wiener process, a random variable drawn from a normal distribution with a mean of 0 and a variance of dt. The starting point of the accumulation process was set to *z* * *a*, where *z* was fixed to an unbiased starting point of 0.5, and *a* represents the upper decision boundary (with 0 representing the lower boundary). To account for the observed RT distributions, which showed a low degree of skew and a strongly decreasing conditional accuracy function, likely induced by the sharp response deadlines, we incorporated a linear boundary collapse mechanism, controlled by an urgency parameter, *u* (model comparisons of initial-decision fits confirmed that adding *u*, and fixing *z*, improved the model fits via lower BIC). The upper boundary at time *t* was defined as *a(t) = a - u*t*, and the lower boundary was defined as *a(t) = 0 + u*t*. A choice and corresponding RT were registered when the accumulated evidence crossed either the upper or lower boundary. We used an accuracy-coding scheme, such that crossing the upper boundary corresponded to a correct response and crossing the lower boundary corresponded to an incorrect response. Finally, a non-decision time parameter, *ter*, was added to the predicted RT

to account for processes unrelated to the decision itself, such as stimulus encoding and motor execution.

Following the initial decision, evidence was allowed to continue accumulating, informing the subsequent confidence judgment. This post-decisional evidence accumulation was modelled with a drift rate (*v2*) that was allowed to differ from the initial drift rate (*v*) (Desender et al., 2022). The post-decisional accumulation continued until a specific criterion was met, with the nature of this criterion differing across the different classes of models we investigated. We evaluated four classes of post-decisional evidence accumulation models, distinguished along two key dimensions: (1) the stopping rule governing the termination of post-decisional accumulation (Time-based vs. Boundary-based) and (2) whether the accumulation process continues from the initial reference frame or restarts in a new reference frame (Single vs. Distinct).

Regarding the stopping rule, in time-based models, post-decisional accumulation terminates after a certain duration. This duration can be fixed, such as during the non-decision time (e.g., "pipeline evidence", Resulaj et al., 2009), set equal to the average observed time of confidence responses, or simply estimated freely (2DSD; Pleskac & Busemeyer, 2010). In Boundary-based models, post-decisional accumulation terminates when the accumulated evidence reaches a collapsing confidence boundary (e.g., Herregods et al., 2023; Moran et al., 2015). Regarding the reference frame, Single-process models assume that post-decisional evidence accumulation continues within the same neural population and reference frame as the initial decision (Grogan et al., 2023). Consequently, the starting point for the confidence judgment is determined by the end point of the initial decision process. Distinct-process models, however, posit that post-decisional evidence accumulation is initiated in a separate neural population, with a new reference frame independent of the initial decision's starting and end points (Fleming et al., 2018). This allows for the possibility that confidence formation could, in principle, run partly in parallel with the initial decision. Another crucial difference with respect to the different reference frames is how differential evidence is translated into absolute evidence, which is further discussed below, in the section on simulating the decision variable.

All post-decisional models included the following parameters: a post-decision drift rate (*v2*), two non-decision time components ($ter2_{no\text{-}CoM}$, $ter2_{CoM}$) to account for differences between change-of-mind and non-change-of-mind trials (as changes of mind required a hand switch), and five confidence criteria (*c1* to *c5*). For convenience, on incorrect trials the post-decision drift rate (*v2*) was multiplied by -1, reversing the direction of accumulation, to reflect the fact that evidence on error trials predominantly supports the incorrect response, which supports metacognitive sensitivity. Note that this is equivalent to keeping the drift rate the same, but flipping the confidence mapping on those trials (i.e., computing confidence conditional on the response).

In the Time-based models, evidence accumulated until a deadline (τ) was reached. Normally distributed noise (σ_τ) around this deadline was included to account for variability in the termination time. In the Boundary-based models, evidence accumulated until it reached one of two collapsing confidence boundaries. For Distinct process models, evidence accumulation started at a new, freely estimated starting point (*z2*) and continued until the timer finished (Time-Distinct model) or it reached either the upper or lower collapsing confidence boundary (Boundary-Distinct model; defined by boundary separation parameter *a2*, and two separate collapse rate parameters, $u2_{up}$, $u2_{down}$). We allowed for negative non-decision times in the Distinct models, consistent with the idea that the initial decision and confidence formation processes can overlap in time. For Single process models, evidence accumulation started at the point where the initial decision boundary was crossed and continued until the timer finished (Time-Single model) or a new set of collapsing confidence

boundaries were reached (Boundary-Single model). These confidence boundaries were defined by parameters $a2_{up}$ and $a2_{down}$ at time 0, and their collapse was controlled by separate urgency parameters ($u2_{up}$, $u2_{down}$).

Finally, the accumulated evidence at the termination of the post-decisional process was mapped onto a discrete six-point confidence rating. This mapping involved adding metacognitive noise (with standard deviation σ_{meta}) to the final evidence value, representing noise in the readout process (Guggenmos, 2022; Shekhar & Rahnev, 2022). The resulting value was then categorized into one of six confidence levels using five freely estimated confidence criteria (*c1* to *c5*). The six confidence levels correspond to "certain", “probably”, “maybe” responses for change-of-mind (ratings 1, 2, and 3) and “maybe”, “probably”, “certain” non-change-of-mind trials (ratings 4, 5, and 6).

Model Fitting Procedure

We employed a two-stage fitting procedure to estimate the parameters of the four post-decisional confidence models. This approach ensured that all models were based on the same pre-decisional mechanisms, allowing us to isolate the effects of different post-decisional processes on confidence formation (simulations confirmed the two-stage fitting could accurately recover models and parameters, see details below and Extended Data Figure 5). In the first stage, we fit the initial decision data using a drift-diffusion model (DDM) with linearly collapsing boundaries. To find the best-fitting parameters for this initial decision model, we minimized a goodness-of-fit metric (*G*2) that compared the observed and model-predicted RT distributions. Specifically, we calculated the *G2* likelihood-ratio statistic as follows:

$$G2 \;=\; 2N \sum_{i,j} p_{i,j}\, log(\frac{p_{i,j}}{\pi_{i,j}}) \qquad (2)$$

where *N* is the total number of observed trials, $p_{i,j}$ and $\pi_{i,j}$ are the observed and simulated proportions of RTs, respectively, that fall within a given quantile bin *i* for each response *j* (correct or incorrect). We used the following quantiles: 0.1, 0.3, 0.5, 0.7, and 0.9, creating 5 bins for correct responses and 5 bins for incorrect responses. The simulated proportions were obtained by simulating the DDM 5000 times for each iteration of the optimization routine. We used Differential Evolution (DEoptim package in R, Mullen et al., 2011) to perform the parameter optimization, running the algorithm for 500 iterations. This procedure was performed separately for each participant and speed condition. The best-fitting parameters (*v*, *a*, *ter*, *u*) from this initial decision model were then fixed in the second stage when fitting the post-decisional models.

In the second stage, we fit the four classes of post-decisional confidence models to the confidence ratings and confidence-RTs. The parameters of the post-decisional models ($v2$, $ter2_{no\text{-}CoM}$, $ter2_{CoM}$, τ, σ_{τ}, $a2$, $z2$, $u2_{up}$, $u2_{down}$, $a2_{up}$, $a2_{lower}$, *c1* to *c5*, σ_{meta}) were estimated by minimizing a composite objective function. This combined three equally weighted goodness-of-fit metrics, each designed to capture a distinct aspect of the behavioural data. Each of the metrics was in the form of a likelihood-ratio statistic, G2, and calculated as specified in formula 2. However, the specific meaning of the indices *i* and *j* varied depending on the metric. A first metric targeted the distribution of confidence-RTs conditional on decision accuracy. Here, *i* indexed the confidence-RT bins (created by the same quantiles as specified above) while *j* indexed the accuracy of the decision. Second, we used the overall proportion of responses for each of the confidence ratings conditional on decision accuracy. Here, *i* indexed the confidence levels (1-6) while *j* indexed the accuracy of the decision. Finally, we calculated the proportion of responses for each confidence rating conditional on five equally-spaced confidence-RT bins to capture the relationship between confidence and confidence-RT. Here, *i* indexed the confidence levels (1-6), while *j* indexed the confidence-RT bin (1-5). The three *G*2 values

were summed to create a composite goodness-of-fit metric that was minimized. We opted for equal weighting of the metrics as we had no a priori reason to prioritize one aspect of the data over another. This approach, using multiple complementary goodness-of-fit metrics, allowed us to constrain the models with different aspects of the behavioural data, ensuring a robust estimation of the post-decision processes.

To compare the fit of the four model classes, we computed the Bayesian Information Criterion (BIC) for each model and each participant, according to the following formula:

$$BIC = G2 + k * log(n) \qquad (3)$$

where k is the number of free parameters, and n is the number of trials (Ratcliff & Tuerlinckx, 2002). Lower BIC values indicate a better fit while taking into account model complexity. In addition to these quantitative metrics, we visually inspected the model fits to assess how well each model captured the key patterns in the behavioural data, including the shapes of the confidence-RT distributions, the relationship between confidence and confidence-RT, and the effects of speed pressure on choice and confidence (see Results and Figure 3).

We validated our model and parameter recovery procedures by simulating data for each set of fitted parameters (1000 trials simulated per 14 participants and 2 conditions) for each of the four models (giving 112 simulations in total), and then fitting each of the four models to these simulated data. The ground-truth model was correctly identified via lowest BIC in 97/112 of these simulations, including 25/28 for the Boundary-Distinct and 28/28 for Boundary-Single. We then took the parameters originally fit to the true data, and correlated them with the parameters recovered from fitting the ground-truth model to simulated data. In general, for each model the recovered parameters highly correlated with the original parameters ($r > .9$), with only lower recovery for some for non-central parameters (e.g. 1st confidence criteria and urgency/collapse-rate for lower confidence boundary in some models). The full model and parameter recovery results can be found in Extended Data Figure 5.

Simulated Decision Variable

To compare the latent decision variable from our models with the neural data (specifically the CPP), we simulated the decision variable's trajectory over time, incorporating additional assumptions and noise sources to better reflect the variability observed in noisy neural scalp recordings and the characteristics of the CPP (Extended Data Figure 2). The decision variable was simulated in epochs ranging from -1s to +3s relative to stimulus onset, with a time step (*dt*) of 0.01s, equivalent to a 100 Hz sampling rate. We simulated 1000 trials for each subject and speed pressure condition. For each trial, we first simulated a pre-stimulus period and an initial non-decision period, assumed to reflect stimulus encoding. During this period, the decision variable was modelled as a noisy mean-reverting Ornstein-Uhlenbeck process (to prevent the DV from hitting the decision boundaries before the evidence began):

$$dx_t = \theta * (\mu - x_t) * dt + \sigma * dW_t \qquad (4)$$

where x_t represents the value of the decision variable at time t, θ is the mean reversion rate (set to 10), μ is the long-term mean to which the process reverts (set to the starting point, 0), σ scales the noise level (set to 0.1), and dW_t is an increment of a Wiener process, drawn from a normal distribution with a mean of 0 and a variance of dt. The duration of the stimulus encoding stage was determined by subtracting a simulated motor execution time from the total non-decision time (*Ter*) estimated in the initial decision model. The motor execution time was assumed to be 0.1s on

average, based on previous work (Kelly et al., 2021), and was drawn for each trial from a uniform distribution ranging +-0.15 s around the expected motor execution time.

Following the encoding stage, the initial decision stage started. Here, differential evidence accumulated according to a standard drift-diffusion process, with drift rate *v* (formula 1). The decision boundaries were transformed so that the starting point of accumulation was 0, rather than *a**z. The boundaries were linearly collapsing, as determined by the urgency parameter *u* from the initial decision model. To approximate the CPP, we computed the absolute value of accumulated differential evidence, i.e., reflecting evidence around zero. This approach is motivated by empirical findings showing that the CPP displays a positive-going increase regardless of the ultimate decision, and is hypothesized to represent the summed activity of two distinct neural populations. Each of these populations encodes evidence for a specific choice option, both with positive polarity, unlike the differential evidence representation typically used in the DDM (Kelly et al., 2021).

The nature of the post-decisional stage depended on the specific process type (Distinct or Single). In Distinct models, a separate evidence accumulation process was initiated with its own starting point. The accumulated evidence in this stage was reflected around this new starting point (*z2*) to represent the absolute value in the reference frame of confidence formation. The simulated trajectories of the initial and post-decisional processes were then summed to generate the final decision variable trajectory. Conversely, Single-process models assumed a continuous accumulation of evidence from the initial decision stage, without a shift in the reflection point. The absolute evidence in these models was calculated throughout the trial by reflecting the accumulated evidence around the original starting point (*z*). Thus, the critical distinction between the Distinct and Single-processes lies in whether the reference frame for evidence accumulation remains fixed throughout the trial and is specified in terms of the original decision (Single) or undergoes a change to form a new, independent process for post-decisional evaluation (Distinct).

The Boundary-Update model used the same fitted parameters as the Boundary-Single model and differed only in terms of how the post-choice accumulation process was simulated. Instead of being a continuation of the accumulation process that determined the initial choice, in Boundary-Update the pre- and post-choice stages of accumulation were simulated with separate signals, with the post-choice signal onsetting at choice-boundary-crossing and the pre-choice process decaying to zero. The post-choice process accumulated post-decision evidence until it crossed a confidence-boundary. This allowed initial-boundary crossing values to affect how close to the confidence boundaries the post-decision process began

Following the post-decisional stage, the level of confidence was determined for all models using the mechanisms described previously. Subsequently, a second non-decision time stage was initiated, representing the time required to execute the confidence response. The duration of this stage was sampled from a uniform distribution centred on the model's fitted mean confidence non-decision time, with a range of ±0.15 s. Separate means were used for change-of-mind trials ($ter2_{CoM}$) and non-change-of-mind trials ($ter2_{no\text{-}CoM}$), to account for the additional motor time required due to changing the response hand. On change-of-mind trials, evidence accumulation was allowed to continue during this confidence non-decision time stage, consistent with the hypothesis that pipeline evidence (i.e., evidence received during the non-decision processes) is continuously integrated even after the initial decision (Resulaj et al., 2009). On non-change-of-mind trials, or upon completion of the confidence non-decision time stage on change-of-mind trials, the accumulated evidence was allowed to decay back towards the starting point. This decay was modelled as a noisy linear decay process:

$$dx = \theta_d * dt + \sigma * dW \qquad (5)$$

where ϑ_d represents the linear decay factor (set to -5; the results were similar for other decay rates). The noise scaling parameter, σ, was the same as that used in the pre-stimulus stage. This decay process ensured that the simulated decision variable gradually returned after the initial response (for very short post-decisional accumulation times) or confidence response had been executed. When plotting the simulated decision variable, the data were smoothed with a 100ms window moving-average (cf. the CPP).

Data Availability

Anonymous data are publicly available on OSF (https://osf.io/4bp96/).

Code Availability

MATLAB code for all analyses is available on GitHub (https://doi.org/10.5281/zenodo.15586067) and the R code for modelling is available on OSF (https://osf.io/f6xyw/).

Acknowledgements

This study was supported by a grant from Horizon 2020 European Research Council Consolidator Grant IndDecision 865474, and grants from the Research Foundation Flanders (1242924N) awarded to L.V., and (G0B0521N) awarded to K.D.

Competing Interests

The authors declare no competing interests.

Author contributions

JPG: Conceptualisation, Methodology, Software, Validation, Formal analysis, Investigation, Data curation, Writing-Original Draft, Writing-Review & Editing, Visualisation, Project administration.

LV: Conceptualisation, Methodology, Software, Validation, Formal analysis, Investigation, Writing-Original Draft, Writing-Review & Editing, Visualisation.

SLM: Investigation, Writing-Review & Editing.

CMC: Investigation, Writing-Review & Editing.

DM: Investigation, Data curation, Writing-Review & Editing.

KD: Conceptualisation, Methodology, Resources, Writing-review & editing, Supervision, Funding Acquisition.

ROG: Conceptualisation, Methodology, Resources, Writing-review & editing, Supervision, Funding Acquisition.

References

Bronfman, Z. Z., Brezis, N., Moran, R., Tsetsos, K., Donner, T., & Usher, M. (2015). Decisions reduce sensitivity to subsequent information. *Proceedings of the Royal Society B: Biological Sciences*, *282*(1810), 20150228. https://doi.org/10.1098/rspb.2015.0228

Bullmore, E. T., Suckling, J., Overmeyer, S., Rabe-Hesketh, S., Taylor, E., & Brammer, M. J. (1999). Global, voxel, and cluster tests, by theory and permutation, for a difference between two groups of structural mr images of the brain. *IEEE Transactions on Medical Imaging*, *18*(1), 32–42. https://doi.org/10.1109/42.750253

Charles, L., & Yeung, N. (2019). Dynamic Sources of Evidence Supporting Confidence Judgments and

Error Detection. *Journal of Experimental Psychology: Human Perception and Performance*, *45*(1), 39–52. https://doi.org/10.1037/xhp0000583.supp

Cisek, P., Puskas, G. A., & El-Murr, S. (2009). Decisions in changing conditions: The urgency-gating model. *Journal of Neuroscience*, *29*(37), 11560–11571. https://doi.org/10.1523/JNEUROSCI.1844-09.2009

Davidson, M. J., Macdonald, J. S. P., & Yeung, N. (2021). Alpha power and stimulus-evoked activity dissociate metacognitive reports of attention , visibility and confidence in a visual detection task. *BioRxiv*. https://doi.org/10.1101/2021.11.23.469669

Delorme, A., & Makeig, S. (2004). EEGLAB: an open source toolbox for analysis of single-trial EEG dynamics including independent component analysis. *Journal of Neuroscience Methods*, *134*, 9–21.

Desender, K., Ridderinkhof, K. R., & Murphy, P. R. (2021). Understanding neural signals of post-decisional performance monitoring: An integrative review. *ELife*, *10*(e67556), 1–21. https://doi.org/10.7554/eLife.67556

Desender, K., Vermeylen, L., & Verguts, T. (2022). Dynamic influences on static measures of metacognition. *Nature Communications*, *13*(1), 1–12. https://doi.org/10.1038/s41467-022-31727-0

Dimigen, O., Sommer, W., Hohlfeld, A., Jacobs, A. M., & Kliegl, R. (2011). Coregistration of eye movements and EEG in natural reading: Analyses and review. *Journal of Experimental Psychology: General*, *140*(4), 552–572. https://doi.org/10.1037/a0023885

Dotan, D., Meyniel, F., & Dehaene, S. (2018). On-line confidence monitoring during decision making. *Cognition*, *171*(February 2017), 112–121. https://doi.org/10.1016/j.cognition.2017.11.001

Dou, W., Afrakhteh, S., & Samaha, J. (2024). Metacognitive Introspection Alters the Dynamics of Pre-Decisional Neural Evidence Accumulation. *BioRxiv*. https://doi.org/10.1101/2024.11.26.625501

Evans, N. J., Hawkins, G. E., & Brown, S. D. (2020). The Role of Passing Time in Decision-Making. *Journal of Experimental Psychology: Learning Memory and Cognition*, *46*(2), 316–326. https://doi.org/10.1037/xlm0000725

Feuerriegel, D., Murphy, M., Konski, A., Mepani, V., Sun, J., Hester, R., & Bode, S. (2022). Electrophysiological correlates of confidence differ across correct and erroneous perceptual decisions. *NeuroImage*, *259*, 119447. https://doi.org/10.1016/j.neuroimage.2022.119447

Fleming, S. M., & Daw, N. D. (2017). Self-evaluation of decision performance: A general Bayesian framework for metacognitive computation. *Psychological Review*, *124*(1), 1–59. https://doi.org/10.1002/smll.))

Fleming, S. M., van der Putten, E. J., & Daw, N. D. (2018). Neural mediators of changes of mind about perceptual decisions. *Nature Neuroscience*, *21*(4), 617–624. https://doi.org/10.1038/s41593-018-0104-6

Gherman, S., & Philiastides, M. G. (2015). Neural representations of confidence emerge from the process of decision formation during perceptual choices. *NeuroImage*, *106*, 134–143. https://doi.org/10.1016/j.neuroimage.2014.11.036

Gherman, S., & Philiastides, M. G. (2018). Human VMPFC encodes early signatures of confidence in perceptual decisions. *ELife*, *7*, 1–28. https://doi.org/10.7554/elife.38293

Grogan, J. P., Rys, W., Kelly, S. P., & O'Connell, R. G. (2023). Confidence is predicted by pre- and post-choice decision signal dynamics. *Imaging Neuroscience*, *1*(August), 1–23.

https://doi.org/10.1162/imag_a_00005

Guggenmos, M. (2022). Reverse engineering of metacognition. *ELife*, *11*, 1–33. https://doi.org/10.7554/eLife.75420

Herding, J., Ludwig, S., von Lautz, A., Spitzer, B., & Blankenburg, F. (2019). Centro-parietal EEG potentials index subjective evidence and confidence during perceptual decision making. *NeuroImage*, *201*, 116011. https://doi.org/10.1016/j.neuroimage.2019.116011

Herregods, S., Le Denmat, P., & Desender, K. (2023). Modelling Speed-Accuracy Tradeoffs in the Stopping Rule for Confidence Judgments. *BioRxiv*, 1–58.

Katsimpokis, D., Hawkins, G. E., & van Maanen, L. (2020). Not all Speed-Accuracy Trade-Off Manipulations Have the Same Psychological Effect. *Computational Brain and Behavior*, *3*(3), 252–268. https://doi.org/10.1007/s42113-020-00074-y

Kayser, J., & Tenke, C. E. (2006). Principal components analysis of Laplacian waveforms as a generic method for identifying ERP generator patterns: I. Evaluation with auditory oddball tasks. *Clinical Neurophysiology*, *117*(2), 348–368. https://doi.org/10.1016/j.clinph.2005.08.034

Kelly, S. P., Corbett, E. A., & O'Connell, R. G. (2021). Neurocomputational mechanisms of prior-informed perceptual decision-making in humans. *Nature Human Behaviour*, *5*(4), 467–481. https://doi.org/10.1038/s41562-020-00967-9

Kelly, S. P., & O'Connell, R. G. (2013). Internal and External Influences on the Rate of Sensory Evidence Accumulation in the Human Brain. *Journal of Neuroscience*, *33*(50), 19434–19441. https://doi.org/10.1523/JNEUROSCI.3355-13.2013

Kiani, R., & Shadlen, M. N. (2009). Representation of confidence associated with a decision by neurons in the parietal cortex. *Science*, *324*(5928), 759–764. https://doi.org/10.1126/science.1169405

Kleiner, M., Brainard, D., Pelli, D., Ingling, A., Murray, R., Broussard, C., & Cornelissen, F. (2007). What's new in Psychtoolbox-3? A free cross-platform toolkit for Psychophysics with Matlab & GNU/Octave. *Perception*, *36*(14), 1. http://www.psychtoolbox.org

Ko, Y. H., Zhou, A., Niessen, E., Stahl, J., Weiss, P. H., Hester, R., Bode, S., & Feuerriegel, D. (2023). Neural correlates of confidence during decision formation in a perceptual judgment task. *BioRXiv*.

Kohl, C., Spieser, L., Forster, B., Bestmann, S., & Yarrow, K. (2020). Centroparietal activity mirrors the decision variable when tracking biased and time-varying sensory evidence. *Cognitive Psychology*, *122*(June), 101321. https://doi.org/10.1016/j.cogpsych.2020.101321

Maris, E., & Oostenveld, R. (2007). Nonparametric statistical testing of EEG- and MEG-data. *Journal of Neuroscience Methods*, *164*(1), 177–190. https://doi.org/10.1016/j.jneumeth.2007.03.024

Matuschek, H., Kliegl, R., Vasishth, S., Baayen, H., & Bates, D. (2017). Balancing Type I error and power in linear mixed models. *Journal of Memory and Language*, *94*, 305–315. https://doi.org/10.1016/j.jml.2017.01.001

Mazor, M., Charles, L., Maimon-Mor, R. O., & Fleming, S. M. (2022). Paradoxical evidence weighting in confidence judgments for detection and discrimination. *PsyArXiv*.

Moran, R., Teodorescu, A. R., & Usher, M. (2015). Post choice information integration as a causal determinant of confidence: Novel data and a computational account. *Cognitive Psychology*, *78*, 99–147. https://doi.org/10.1016/j.cogpsych.2015.01.002

Mullen, K. M., Ardia, D., Gil, D. L., Windover, D., & Cline, J. (2011). DEoptim: An R package for global optimization by differential evolution. *Journal of Statistical Software*, *40*(6), 1–26. https://doi.org/10.18637/jss.v040.i06

Murphy, P. R., Boonstra, E., & Nieuwenhuis, S. (2016). Global gain modulation generates time-dependent urgency during perceptual choice in humans. *Nature Communications*, *7*(May), 1–14. https://doi.org/10.1038/ncomms13526

Murphy, P. R., Robertson, I. H., Harty, S., & O'Connell, R. G. (2015). Neural evidence accumulation persists after choice to inform metacognitive judgments. *ELife*, *4*, e11946. https://doi.org/10.7554/eLife.11946

O'Connell, R. G., & Kelly, S. P. (2021). Neurophysiology of Human Perceptual Decision-Making. *Annual Review of Neuroscience*, *44*(1), 495–516. https://doi.org/10.1146/annurev-neuro-092019-100200

Ouyang, G., Sommer, W., & Zhou, C. (2015). A toolbox for residue iteration decomposition (RIDE)-A method for the decomposition, reconstruction, and single trial analysis of event related potentials. *Journal of Neuroscience Methods*, *250*, 7–21. https://doi.org/10.1016/j.jneumeth.2014.10.009

Pleskac, T. J., & Busemeyer, J. R. (2010). Two-stage dynamic signal detection: A theory of choice, decision time, and confidence. *Psychological Review*, *117*(3), 864–901. https://doi.org/10.1037/a0019737

Ratcliff, R., & Tuerlinckx, F. (2002). Estimating parameters of the diffusion model: Approaches to dealing with contaminant reaction times and parameter variability. *Psychonomic Bulletin and Review*, *9*(3), 438–481. https://doi.org/10.3758/BF03196302

Resulaj, A., Kiani, R., Wolpert, D. M., & Shadlen, M. N. (2009). Changes of mind in decision-making. *Nature*, *461*(7261), 263–266. https://doi.org/10.1038/nature08275

Rogge, J., Jocham, G., & Ullsperger, M. (2022). Motor cortical signals reflecting decision making and action preparation. *NeuroImage*, *263*(October), 119667. https://doi.org/10.1016/j.neuroimage.2022.119667

Rollwage, M., Loosen, A., Hauser, T. U., Moran, R., Dolan, R. J., & Fleming, S. M. (2020). Confidence drives a neural confirmation bias. *Nature Communications*, *11*(1). https://doi.org/10.1038/s41467-020-16278-6

Shekhar, M., & Rahnev, D. (2022). How do humans give confidence? A comprehensive comparison of process models of metacognition. *PsyArXiv*. https://doi.org/10.31234/osf.io/cwrnt

Steinemann, N. A., O'Connell, R. G., & Kelly, S. P. (2018). Decisions are expedited through multiple neural adjustments spanning the sensorimotor hierarchy. *Nature Communications*, *9*(3627), 1–13. https://doi.org/10.1038/s41467-018-06117-0

Tagliabue, C. F., Veniero, D., Benwell, C. S. Y., Cecere, R., Savazzi, S., & Thut, G. (2019). The EEG signature of sensory evidence accumulation during decision formation closely tracks subjective perceptual experience. *Scientific Reports*, *9*(1), 4949. https://doi.org/10.1038/s41598-019-41024-4

Talluri, B. C., Urai, A. E., Bronfman, Z. Z., Brezis, N., Tsetsos, K., Usher, M., & Donner, T. H. (2021). Choices change the temporal weighting of decision evidence. *Journal of Neurophysiology*, *125*(4), 1468–1481. https://doi.org/10.1152/jn.00462.2020

Talluri, B. C., Urai, A. E., Tsetsos, K., Usher, M., Donner, T. H., Talluri, B. C., Urai, A. E., Tsetsos, K.,

Usher, M., & Donner, T. H. (2018). Confirmation Bias through Selective Overweighting of Choice-Consistent Evidence Report. *Current Biology*, 1–8. https://doi.org/10.1016/j.cub.2018.07.052

Twomey, D. M., Murphy, P. R., Kelly, S. P., & O'Connell, R. G. (2015). The classic P300 encodes a build-to-threshold decision variable. *European Journal of Neuroscience*, *42*(1), 1636–1643. https://doi.org/10.1111/ejn.12936

Van Den Berg, R., Anandalingam, K., Zylberberg, A., Kiani, R., Shadlen, M. N., & Wolpert, D. M. (2016). A common mechanism underlies changes of mind about decisions and confidence. *ELife*, *5*(FEBRUARY2016), 1–21. https://doi.org/10.7554/eLife.12192

Vickers, D. (1979). *Decision Processes in Visual Perception*. Academic Press.

Visalli, A., Montefinese, M., Viviani, G., Finos, L., Vallesi, A., & Ambrosini, E. (2024). lmeEEG: Mass linear mixed-effects modeling of EEG data with crossed random effects. *Journal of Neuroscience Methods*, *401*(June 2023), 109991. https://doi.org/10.1016/j.jneumeth.2023.109991

Walsh, K., McGovern, D. P., Dully, J., Kelly, S. P., & O'Connell, R. G. (2024). Prior probability cues bias sensory encoding with increasing task exposure. *ELife*, *12*, 1–24. https://doi.org/10.7554/eLife.91135

Watson, A. B. ., & Pelli, D. (1983). QUEST: A Bayesian adaptive psychophysical method. *Perception & Psychophysics*, *33*(2), 113–120.

Xue, K., Zheng, Y., Rafiei, F., & Rahnev, D. (2023). The timing of confidence computations in human prefrontal cortex. *Cortex*, *168*, 167–175. https://doi.org/10.1016/j.cortex.2023.08.009

Yu, S., Pleskac, T. J., & Zeigenfuse, M. D. (2015). Dynamics of Postdecisional Processing of Confidence. *Journal of Experimental Psychology General*, *144*(2), 489–510. https://doi.org/10.1037/a0039293